Hindawi
Advances in Civil Engineering
Volume 2019, Article ID 2130943, 9 pages
https://doi.org/10.1155/2019/2130943

Research Article

Analysis of the Thermal Characteristics of Surrounding Rock in Deep Underground Space

Liu Chen, Jiangbo Li, Fei Han, Yu Zhang, Lang Liu, and Bo Zhang

Energy School, Xi'an University of Science and Technology, Yanta Road, Xi'an 710054, China

Correspondence should be addressed to Lang Liu; liulang@xust.edu.cn

Received 20 September 2018; Accepted 11 December 2018; Published 16 January 2019

Guest Editor: Zhanguo Ma

With the development of society, the economy, and national security, the exploitation of deep underground space has become an inevitable trend in human society. However, high-temperature-related problems occur in deep underground spaces. The high temperature of deep underground space is essentially influenced by the thermal characteristics of the surrounding rock. According to the mathematical model of heat transfer of the surrounding rock in deep underground space, similar criteria numbers are established. Experiments were carried out to investigate the thermal characteristics of the surrounding rock. The distribution characteristics of temperature were determined by the Fourier number (F_o) and Biot number (B_i), and the effects of heat transfer time, airflow velocities, and air temperature and radial displacement on the distribution characteristics of temperature were studied. The results indicate that the surrounding rock temperature decreases with long heat transfer times, high airflow velocities, and low air temperatures.

1. Introduction

As an important part of urban space resources, underground space is an important way to promote urban sustainable development ability [1, 2]. These uses of underground space include the installation of transportation infrastructure, public utilities, disposal of waste, energy utilization facility, storage of substances, and exploitation of minerals [3–9]. Resources in shallow underground spaces have gradually become exhausted. Therefore, exploiting deep underground space is becoming increasingly important [10].

The challenges associated with deep underground spaces include high temperatures, which are harmful to human health, and decreased production efficiency [11, 12]. In deep underground space, the major source of high temperatures is geothermal energy. Geothermal energy continuously transfers from surrounding rocks to deep underground spaces. It is essential to understand the thermal characteristics of surrounding rock in deep underground spaces. Many researchers have examined the thermal characteristics of surrounding rock by theoretical, experimental, and numerical modelling approaches. The unsteady heat transfer equation of the rocks surrounding deep roadways with constant air volume was solved using a variable separation approach. The solution was an infinite series including Bessel functions [13]. Numerical simulation was utilized to study the effect of heat generated after burying radioactive waste on the stability of underground space and the surrounding rock strata for 16 years at a constant heat flux [14]. The random temperature fields of a tunnel in a cold region were obtained by numerical simulation and analysed with stochastic boundary conditions and random rock properties [15]. The steady heat transfer of surrounding rocks in roadway ventilation was numerically analysed. The heat flux was approximately uniformly distributed in a ring shape. The heat flux of the rock near the roadway wall was greater than that in the far side roadway wall [16].

The heat characteristics of the surrounding rock in subway tunnels were analysed by experimental testing for 17 years. The heat characteristics of the surrounding rock varied with depth, and heat storage and release are noted [17]. Heat transfer characteristics in a single rock fracture were

investigated. The experimental results indicated that the roughness of rock improves overall heat transfer, whereas lithology has little influence on heat transfer [18].

Although extensive research on the heat characteristics of surrounding rock in deep underground spaces has been conducted using theoretical, numerical, and field test methods, there are only a few experimental studies, most of which are focused on steady heat transfer rather than unsteady heat transfer.

This study aims at experimentally investigating the unsteady thermal characteristics of surrounding rock in deep underground space. The thermal properties of surrounding rocks and boundary conditions of different deep underground spaces have significant differences. Similarity experiments were carried out to investigate the thermal characteristics of surrounding rock, and the effects of the main parameters on the temperature distribution characteristics are discussed.

2. Heat Transfer Model and Similar Criteria of Surrounding Rock in Deep Underground Space

2.1. Basic Assumptions. To model the heat transfer of surrounding rock in deep underground space, the following simplified assumptions are made:

(1) The inner boundary of the surrounding rock is a hollow cylinder with an infinite outer diameter

(2) The surrounding rock mass is homogeneous and isotropic

(3) The seepage effect of water in the surrounding rock is negligible

(4) The initial temperature of the surrounding rock is equivalent to its original rock temperature

2.2. Mathematical Model. Based on the above assumptions, which conform to one-dimensional unsteady thermal conduction, the mathematical description of cylindrical coordinate form regardless of the variation in the axial temperature of the surrounding rock is adopted.

The mathematical equations governing the heat transfer of surrounding rock in deep underground space are shown as follows:

$$\frac{\partial \mathrm{T}}{\partial \tau} = a\left(\frac{\partial^2 T}{\partial r^2} + \frac{1}{r}\frac{\partial T}{\partial r}\right). \tag{1}$$

Initial condition:

$$T(r,\tau)|_{\tau=0} = T_0. \tag{2}$$

Boundary condition:

$$\begin{cases} \lambda \dfrac{\partial T}{\partial r}\Big|_{r=r_0} = h\left(T - T_{\mathrm{f}}\right), & \tau > 0. \\ T\big|_{r\longrightarrow\infty} = T_0, \end{cases} \tag{3}$$

2.3. Similarity Analysis. Dimensionless equation (1) is obtained where $\theta_0 = T_0 - T_{\mathrm{f}}$ is selected as the temperature measuring scale, the radial radius r_0 is selected as the length measuring scale, ${r_0}^2/\alpha_0$ is selected as the time measuring scale, the average thermal conductivity coefficient λ_0 is selected as the thermal conductivity coefficient measuring scale, the average thermal diffusivity α_0 is selected as thermal diffusivity measuring scale, and the average convective heat transfer coefficient h_0 is selected as the convective heat transfer coefficient of surrounding rock and the airflow measuring scale.

Dimensionless equation (4) can be expressed as follows:

$$\frac{\theta_0}{r_0^2/a_0}\frac{\partial\left(\theta/\theta_0\right)}{\partial\left(a_0\tau/r_0^2\right)} = a_0\frac{a}{a_0}\left[\frac{1}{r_0}\frac{1/r}{1/r_0}\frac{\theta_0}{r_0}\frac{\partial\left(\theta/\theta_0\right)}{\partial\left(r/r_0\right)} + \frac{\theta_0}{r_0^2}\frac{\partial^2\left(\theta/\theta_0\right)}{\partial\left(r/r_0\right)^2}\right]. \tag{4}$$

The dimensionless temperature, dimensionless radius, and dimensionless thermal diffusion coefficient are given as follows:

$$\begin{aligned} \Theta &= \frac{\theta}{\theta_0}, \\ R &= \frac{r}{r_0}, \\ A &= \frac{a}{a_0}. \end{aligned} \tag{5}$$

Ignoring the change of thermal properties of surrounding rocks with temperature, A is equal to 1; then Equation (4) can be converted into

$$\frac{a_0}{\theta_0}\frac{\partial\Theta}{\partial\left(a_0\tau/r_0^2\right)} = \frac{a_0\theta_0}{r_0^2}\left(\frac{1}{R}\frac{\partial\Theta}{\partial R} + \frac{\partial^2\Theta}{\partial R^2}\right). \tag{6}$$

The initial conditions can be converted as follows:

$$\begin{aligned} \frac{a_0\tau}{r_0 2} &= 0, \\ \Theta &= 1. \end{aligned} \tag{7}$$

The boundary conditions can be converted to

$$\begin{cases} R = 1, \quad \lambda_0\dfrac{\theta_0}{r_0}\dfrac{\partial\Theta}{\partial R} = h_0\theta_0\Theta, & \dfrac{a_0\tau}{r_0^2} > 0. \\ R \longrightarrow \infty \quad \dfrac{\partial\Theta}{\partial R} = 0, \end{cases} \tag{8}$$

The dimensionless equations governing the heat transfer of surrounding rock in deep underground space are shown as follows:

$$\frac{\partial\Theta}{\partial\left(F_{\mathrm{o}}\right)} = \frac{1}{R}\frac{\partial\Theta}{\partial R} + \frac{\partial^2\Theta}{\partial R^2}. \tag{9}$$

The dimensionless initial condition is as follows:

$$F_o = 0, \quad \Theta = 1. \tag{10}$$

The dimensionless boundary condition is as follows:

$$\begin{cases} R = 1, & \dfrac{\partial \Theta}{\partial R} = B_i \Theta, \\ & F_o > 0. \\ R \longrightarrow \infty, & \dfrac{\partial \Theta}{\partial R} = 0, \end{cases} \tag{11}$$

From the derivation of the above dimensionless Equation (9), the dimensionless initial condition (12), and the dimensionless boundary conditions (11), it can be seen that the dimensionless temperature Θ of surrounding rock is a function of F_o, B_i, and R, that is,

$$\Theta = f(F_o, B_i, R). \tag{12}$$

Therefore, the conclusion is obtained as follows: the Fourier number F_o and Biot number B_i are the similar criteria numbers of surrounding rock in deep underground space.

3. Experimental Method

3.1. Prototype and Model. Surrounding rock in a deep underground tunnel was taken as the prototype. The depth of the deep underground tunnel centre is 965 m. Taking the rock surrounding a tunnel as a three-dimensional model, it was simplified as cuboids. The tunnel space is located in the middle of the surrounding rock, and the equivalent diameter of the tunnel is 5 m. The surrounding rock of the prototype is 25 m long, 25 m wide, and 62.5 m high. A 1 : 25 scale model was built to carry out small-scale model experiments to investigate the thermal characteristics of surrounding rock in deep underground space.

3.2. Experimental Device. Figure 1 shows the schematic diagram of the experimental set up. The experimental set up consists of a surrounding rock model, a space model, air conditioning equipment, a thermal boundary system, and a data acquisition system. The surrounding rock model is enclosed by stainless steel and covered with an insulating layer to ensure a constant boundary temperature. The air-conditioning equipment, which consisted of cooling coil, an electric heater, a steam humidifier, and a process fan, is able to supply air under various conditions to the space model. Figure 2 is a photograph of the air conditioning equipment. The thermal boundary system is composed of a heating belt and a temperature controller that are uniformly attached to the outer wall of the surrounding rock to guarantee the fixed thermal boundary temperature requirements were satisfied. The data acquisition system collects and controls the air temperature, air humidity, air speed, and internal temperature of the surrounding rock. There are arranged temperature measuring points in the surrounding rock. The layout of the measuring points in the surrounding rock model is shown in Figure 3. Each temperature in radius displacement r is taken from the average of the vertical and horizontal direction temperature. The photograph of the experimental set up is shown in Figure 4.

The measurement parameters used for the experimental set up and the type and accuracy of the sensor are shown in Table 1. The sensor position is shown in Figures 1 and 3.

3.3. Experimental Design. The experimental model should be guaranteed to be equal to Fourier number F_o, Biot number B_i and the single value condition of the prototype. The single value condition is the initial rock temperature, the constant temperature boundary of the infinite surrounding rock, and the convection heat transfer boundary of the space. The initial rock temperature and boundary temperature of the model are the same as those of the prototype, the inlet air temperature, and inlet air humidity. The humidity in deep underground space is generally high; accordingly, the relative humidity of the inlet air of space in this experiment is constant at 80%. Air enters the space model from the air-conditioning equipment through a section of horizontal pipe, and the length of the horizontal pipe is 40 times the diameter of the space, so it can be considered that the air in the underground space model is in the fully developed area of flow [19].

3.4. Thermal Properties of Surrounding Rocks. The thermal properties of the surrounding rock in deep underground space are less affected by pressure variations and temperature variations, so the thermal properties of the surrounding rock can be considered constant. A similar surrounding rock material with a mixture of cement, expanded perlite, quartz sand, aluminium powder, and water was formed. The thermal properties of the surrounding rocks measured by the apparatus in the experiment are shown in Table 2.

As shown in Table 2, the thermal properties of the surrounding rock in the experimental model are smaller than the properties of the artificial rock. This is because r in the experimental model is small compared to r in the prototype, so with F_o being equal, smaller thermal conductivity is used in the experimental model.

3.5. Convective Heat Transfer Coefficient. In this experiment, the convective heat transfer coefficient was calculated. The following method was used to calculate the convective heat transfer coefficient.

The heat gain of air in space is as follows:

$$Q_1 = G(i_2 - i_1). \tag{13}$$

The convective heat transfer between the wall surface of the space and the air is as follows:

$$Q_2 = h(T_w - T_p)A_1. \tag{14}$$

Ignoring the heat loss from airflow, Q_1 should be equal to Q_2. The convective heat transfer coefficient h of the wall surface of the space and the air can be obtained as follows:

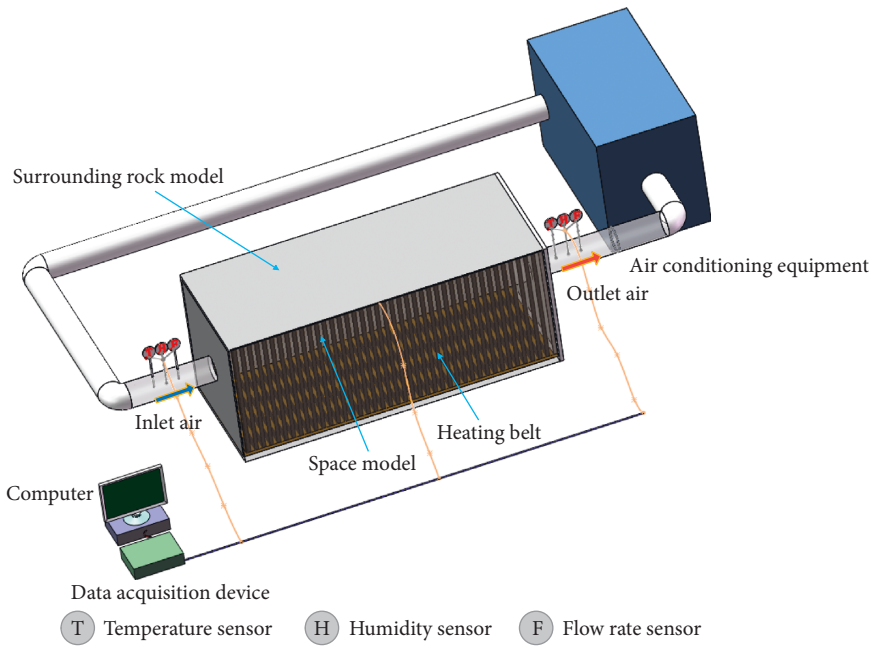

Figure 1: Schematic diagram of the experimental set up.

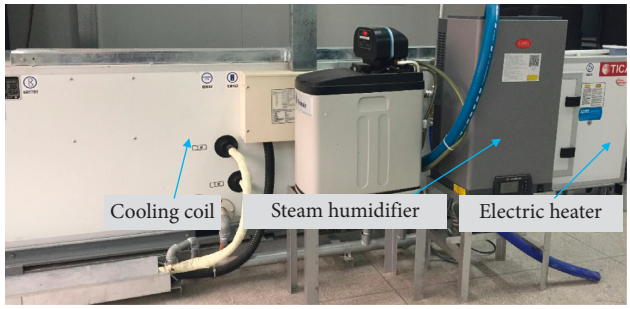

Figure 2: Photograph of the air-conditioning equipment.

$$h = \frac{G(i_2 - i_1)}{A(T_w - T_p)}. \quad (15)$$

4. Results and Discussion

4.1. Fourier Number F_o^*. The experimental conditions were as follows: original rock temperature, 50°C; inlet air temperature, 12°C; inlet air relative humidity, 80%; and inlet airflow velocity, 3.5 m/s. The dimensionless temperature distribution of the surrounding rock was tested by varying F_o' from 0 to 0.4.

Figure 5 shows that the higher the F_o^* is, the lower the Θ is. When F_o^* is greater than 0.3, the dimensionless temperature of the surrounding rock remained substantially constant. As shown in Figure 5, three stages can be distinguished in terms of change in the dimensionless temperature: initial stage ($F_o^* = 0$–0.15), transition stage ($F_o^* = 0.15$–0.3), and stabilization stage ($F_o^* > 0.3$). The influence of F_o^* on Θ mainly occurs in the initial stage, while F_o^* has an influence in the stabilization stage. This indicates that when F_o^* is greater than 0.3, the dimensionless temperature distribution of the surrounding rock depends on R and B_i independently of F_o^*. Therefore, when F_o^* is greater than 0.3, the unsteady heat transfer model of surrounding rock in deep underground space could be simplified to a steady heat transfer model for simplification of the calculations.

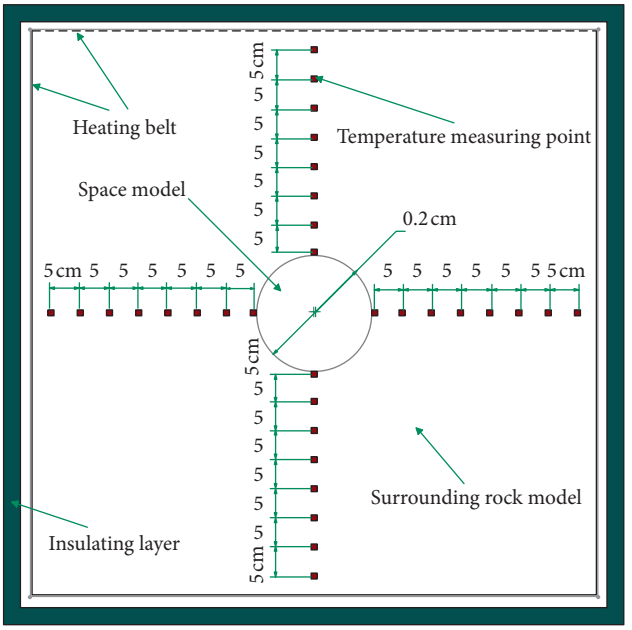

Figure 3: Layout of measuring points in the surrounding rock model.

4.2. Biot Number B_i. The experimental conditions were as follows: original rock temperature, 30°C; inlet air

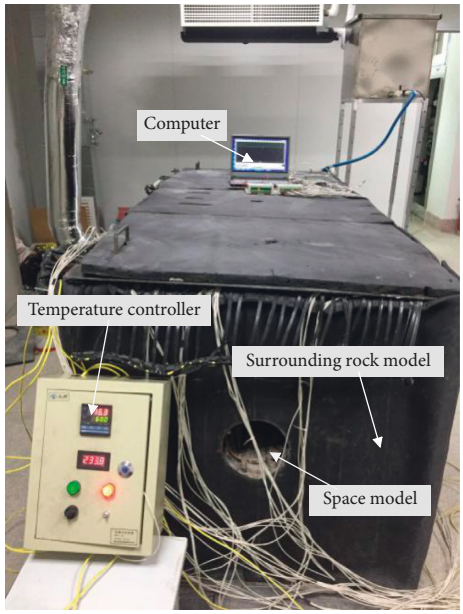

Figure 4: Photograph of the experimental set up.

Table 1: Measured parameters.

Measured parameter	Type	Measurement range	Accuracy
Temperature	PT 100	−40°C~150°C	±0.5°C
Relative humidity	Capacitive	0%~100% RH	±2%
Airflow velocity	Hot wire	0 m/s~15 m/s	±0.2 m/s

Table 2: Thermal properties of surrounding rocks.

Density (kg/m³)	Specific heat capacity (kJ/(kg·k))	Thermal conductivity W/(m·K)
772	0.804	0.139

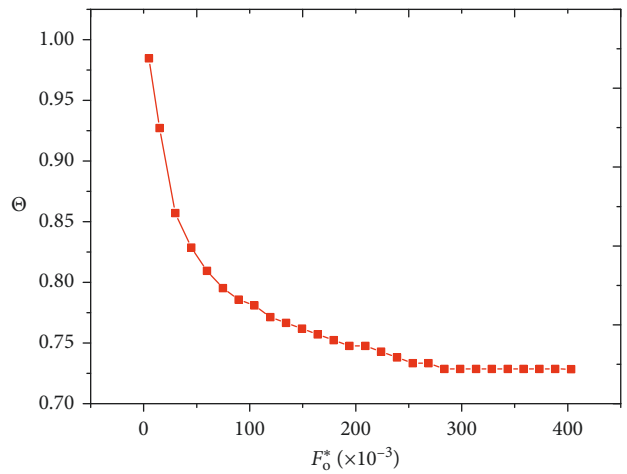

Figure 5: Effect of F_o^* on Θ.

temperature, 15°C; inlet air relative humidity, 80%; and inlet airflow velocity, 3.5 m/s ($B_i = 9.87$) and 6.0 m/s ($B_i = 15.2$). The dimensionless temperature distribution of the surrounding rock was tested by varying F_o.

As shown in Figure 6, comparing the dimensionless temperatures under two different B_i, the results show that Θ decreases with increasing B_i, but the influence of B_i decreases with increasing dimensionless displacement R. A major reason for the decrease in Θ is that higher B_i leads to a thinner boundary layer. Since convective heat transfer between the internal surface of surrounding rock and air was strengthened, the closer the measuring point to the internal surface is, the lower the Θ is.

It can be seen in Figure 6 that there is little effect on Θ as F_o increases, and when F_o is greater than 0.355, B_i has no substantial effect on Θ. Furthermore, as a result, when F_o is greater than 0.355, the unsteady heat transfer model of surrounding rock in deep underground space is significantly not influenced by convection heat transfer boundary conditions.

4.3. Radial Displacement R. The experimental conditions were as follows: original rock temperature, 50°C; inlet air temperature, 12°C; inlet air relative humidity, 80%; and inlet airflow velocity, 3.5 m/s. The dimensionless temperature distribution of the surrounding rock was tested by varying R.

Figure 7 shows that when F_o is equal to 0, the heat transfer starts, and the temperature of the surrounding rock maintains the original rock temperature in all radial displacements. The results verified the accuracy of the experiment.

Figure 7 shows the trends of Θ against R. When R changes from 1.5 to 4.5, Θ increases. The greater the F_o is, the higher the temperature difference between measured points or the temperature gradient is. Θ remains almost constant and equal to 1 when R is equal to 4.5. A major reason for the increase in Θ is that the original temperature field of the surrounding rock is disturbed by air from near R to far R. The wall surface near the underground space ($R = 1.5$) is affected by the ventilation of the deep underground space, and the temperature is slightly lower, while the bottom of the surrounding rock ($R = 4.5$) is affected by the original rock temperature, and the temperature is higher.

As shown in Figure 7, the temperature gradient decreases with increasing R; that is, the heat flux density decreases with increasing R according to Fourier's law. This is because the geothermal heat in the deep part of the surrounding rock continuously transfers to deep underground space while the airflow passes. The airflow has not yet been able to disturb the temperature field there, or the heat carried by the airflow is less than the heat transmitted to it; that is, the temperature range of the surrounding rock that can be spread into the underground space is from near R to far R.

As shown in Figure 7, the curve of an F_o value of 0.403 and the curve of an F_o value of 0.470 nearly overlap. The results show that when F_o is more than 0.403, the dimensionless temperature distribution tends to be stable, as does the heat flux density distribution.

4.4. Inlet Air Temperature T_f. The experimental conditions were as follows: original rock temperature, 40°C; inlet air relative humidity, 80%; and inlet airflow velocity, 5 m/s. The dimensionless temperature distribution of the surrounding rock was tested by varying the inlet air temperature from 16°C to 25°C.

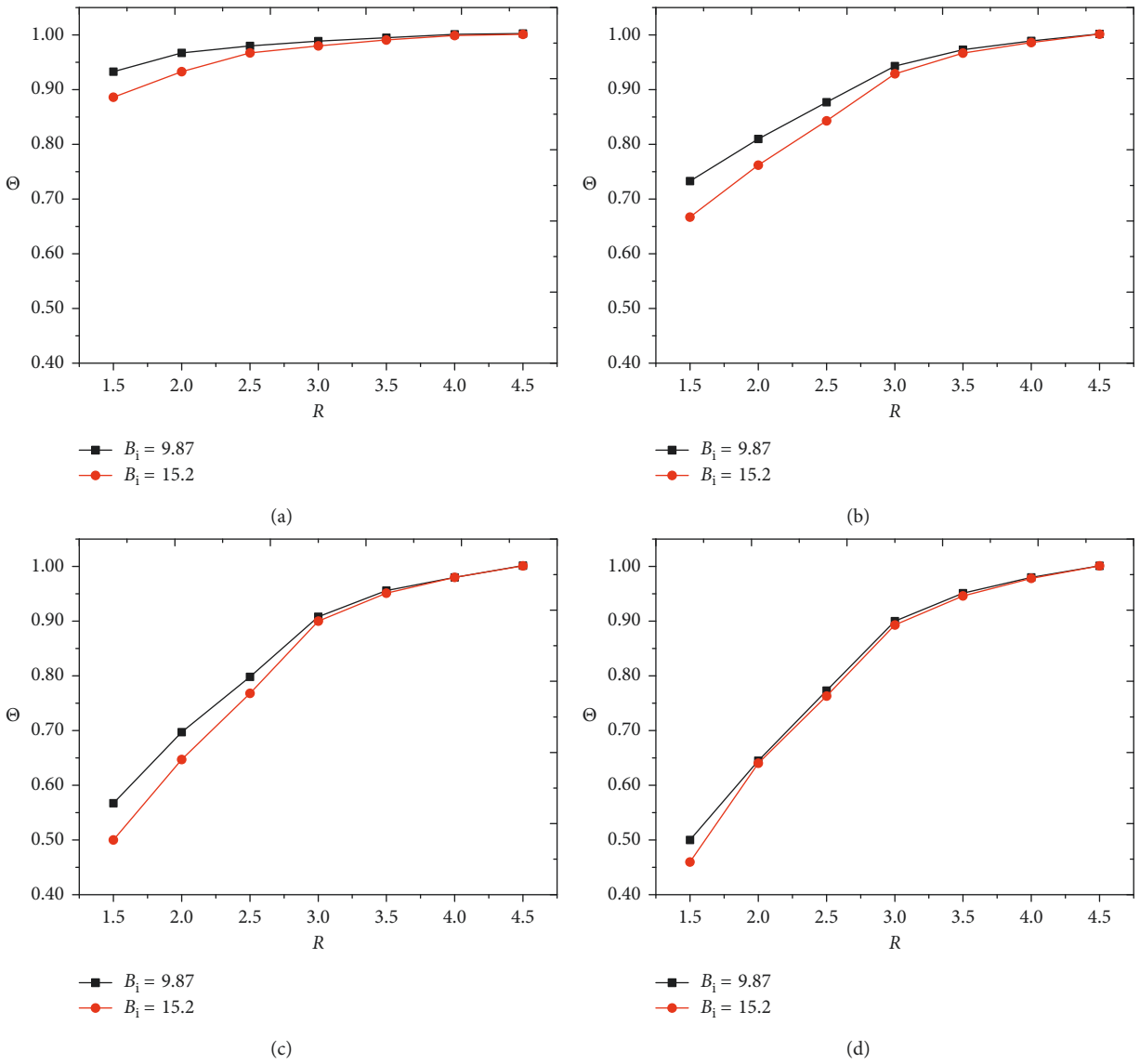

Figure 6: Effect of B_i on Θ. (a) $F_o = 0.067$. (b) $F_o = 0.201$. (c) $F_o = 0.268$. (d) $F_o = 0.355$.

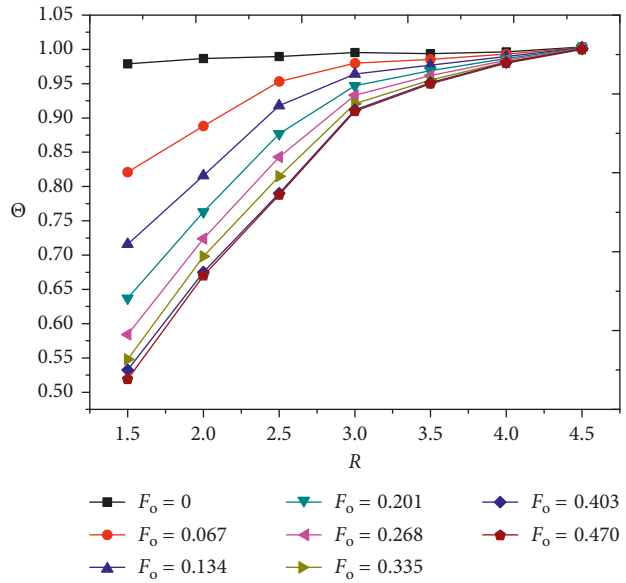

Figure 7: Effect of R on Θ.

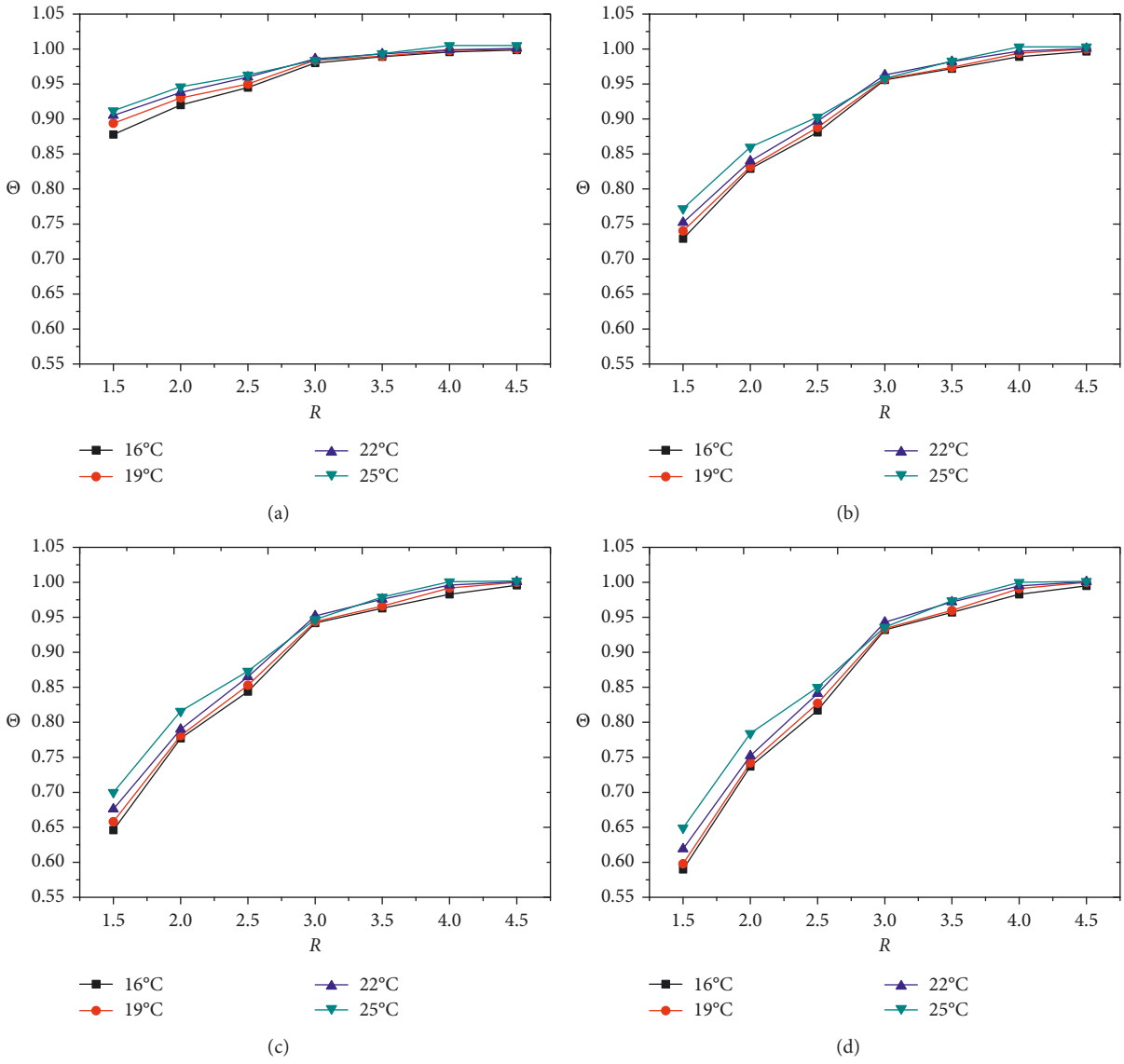

Figure 8: Effect of t_f on Θ. (a) $F_o = 0.067$. (b) $F_o = 0.201$. (c) $F_o = 0.268$. (d) $F_o = 0.355$.

Figure 8 shows the trends of Θ against T_f. When T_f changes from 16°C to 25°C, Θ increases. A major reason for the increase in Θ is that higher T_f leads to a smaller temperature difference between the internal surface of surrounding rock and air, which decreases heat convection.

As shown in Figure 8, T_f affected the closer measuring points more than the further measuring points. When R was equal to 4.5, Θ was nearly equivalent to 1.0 with any value of F_o. This also indicates that the influence of air temperature on the heat transfer range is negligible.

5. Conclusions

(a) The heat transfer between surrounding rock and deep underground space is a complicated, nonstationary process. A 1-dimensional nonstationary heat transfer model was established to model the heat transfer of surrounding rock and deep underground space. The temperature distribution of the surrounding rock was a function of the radial displacement (R), Biot number (B_i), and Fourier number (F_o) by dimensional analysis.

(b) Experiments were carried out to investigate the thermal characteristics of the surrounding rock. In this experiment, Fourier number (F_o) and Biot number (B_i) were adopted as the criteria of similarity, and the model was made at a 1/25 geometric scale. Through simulation experiments, the temperature field of the surrounding rock is obtained, and the effects of F_o, B_i, R, and T_f on Θ are analysed.

(c) The experimental results indicate that three stages can be distinguished in terms of change in dimensionless temperature: initial stage ($F_o' = 0$–0.15), transition stage ($F_o' = 0.15$–0.3), and stabilization stage ($F_o' > 0.3$). To facilitate engineering applications, the nonstationary heat transfer of surrounding

rock in deep underground space could be simplified as stationary heat transfer in the stabilization stage. When R is less than or equal to 4.0, the higher the F_o and B_i are, the lower the dimensionless temperature with the same R is, while the higher the T_f is, the higher the dimensionless temperature with the same R is. When R is equal to 4.5, Θ is nearly equivalent to 1.0 with any value of F_o, B_i, and T_f. Thus, when F_o is less than or equal to 0.47, and R is greater than or equal to 4.5, and the temperature field of the surrounding rock is less affected by the underground space.

Nomenclature

A: Dimensionless thermal diffusivity (α/α_0)
A_1: Internal surface area of surrounding rock (m^2)
B_i: Biot number (hr_0/λ)
F_o: Fourier number with the feature size of r_0 ($\alpha\tau/r_0^2$)
F_o^*: Fourier number with the feature size of r ($\alpha\tau/r^2$)
G: Air mass flow rate (kg/s)
h: Convective heat transfer coefficient (W/(m^2·K))
h_0: Average convective heat transfer coefficient (W/(m^2·K))
i: Enthalpy (kJ/kg)
Q: Heat gain (kW)
R: Dimensionless radial displacement (r/r_0)
r: Radius displacement (m)
r_0: Space radius (m)
T: Temperature (°C)
T_f: Air temperature (°C)
T_0: Initial temperature (°C)
T_w: Wall temperature (°C)
T_p: Average temperature of the air (($T_2 - T_1$)/2) (°C)

Greek Symbols

Θ: Dimensionless temperature (($T - T_f$)/($T_0 - T_f$))
α: Thermal diffusivity (m^2/s)
α_0: Average thermal diffusivity (m^2/s)
θ_0: Temperature measuring scale ($T_0 - T_f$) (°C)
λ: Thermal conductivity (W/(m·K))
λ_0: Average thermal conductivity (W/(m·K))
τ: Time (s).

Subscript

1: Inlet air
2: Outlet air.

Data Availability

All the original data used to support the findings of this study are shown in the figures.

Conflicts of Interest

The authors declare that they have no conflicts of interest.

Acknowledgments

This study was supported by the National Natural Science Foundations of China (Nos. 51404191, 51504182, 51674188, and 51774229), Shaanxi Innovative Talents Cultivate Program-New-Star Plan of Science and Technology (2018KJXX-083), Natural Science Basic Research Plan of Shaanxi Province of China (No. 2015JQ5187), Scientific Research Program funded by the Shaanxi Provincial Education Department (No. 15JK1466), China Postdoctoral Science Foundation (No. 2015M582685), and Outstanding Youth Science Fund of Xi'an University of Science and Technology (No. 2018YQ2-01).

References

[1] X. Wang, F. Zhen, X. Huang, M. Zhang, and Z. Liu, "Factors influencing the development potential of urban underground space: structural equation model approach," *Tunnelling and Underground Space Technology*, vol. 38, no. 3, pp. 235–243, 2013.

[2] B. Uliasz-Misiak and A. Przybycin, "Present and future status of the underground space use in Poland," *Environmental Earth Sciences*, vol. 75, no. 22, p. 1430, 2016.

[3] M. Wang, L. Liu, L. Chen, X. Zhang, B. Zhang, and C. Ji, "Cold load and storage functional backfill for cooling deep mine," *Advances in Civil Engineering*, vol. 2018, Article ID 5435214, 8 pages, 2018.

[4] D. Evans, M. Stephenson, and R. Shaw, "The present and future use of 'land' below ground," *Land Use Policy*, vol. 26, pp. S302–S316, 2009.

[5] N. Bobylev, "Mainstreaming sustainable development into a city's master plan: a case of urban underground space use," *Land Use Policy*, vol. 26, no. 4, pp. 1128–1137, 2009.

[6] C. D. F. Rogers, H. Parker, R. Sterling et al., "Sustainability issues for underground space in urban areas," *Urban Design & Planning*, vol. 165, no. 4, pp. 241–254, 2012.

[7] S. A. Alkaff, S. C. Sim, and M. N. Ervina Efzan, "A review of underground building towards thermal energy efficiency and sustainable development," *Renewable and Sustainable Energy Reviews*, vol. 60, pp. 692–713, 2016.

[8] Z. Yujiao, L. Ruoyao, J. Changfa, H. Chao, Z. Bo, and L. Lang, "Parametric study and design of an earth-air heat exchanger using model experiment for memorial heating and cooling," *Applied Thermal Engineering*, vol. 148, no. 2, pp. 838–845, 2019.

[9] L. Lang, F. Zhiyu, Q. Chongchong, Z. Bo, G. Lijie, and K. I.-I. L. Song, "Numerical study on the pipe flow characteristics of the cemented paste backfill slurry considering hydration effects," *Powder Technology*, vol. 343, pp. 454–464, 2019.

[10] P. G. Ranjith, J. Zhao, M. Ju, R. V. S. De Silva, T. D. Rathnaweera, and A. K. M. S. Bandara, "Opportunities and challenges in deep mining: a brief review," *Engineering*, vol. 3, no. 4, pp. 546–551, 2017.

[11] F. Winde, F. Kaiser, and E. Erasmus, "Exploring the use of deep level gold mines in South Africa for underground pumped hydroelectric energy storage schemes," *Renewable and Sustainable Energy Reviews*, vol. 78, pp. 668–682, 2017.

[12] F. H. V. Glehn, R. Hemp, and R. C. Funnell, "Numerical modelling of heat flow in mines," *South African Journal of Science*, vol. 98, no. 9, pp. 485–490, 2002.

[13] Y. Wang, G. Zhou, L. Wu, Y. Zhou, and Y. Lu, "An analytical study of unsteady heat transfer in the rock surrounding a deep airway," *International Journal of Mining Science and Technology*, vol. 22, no. 3, pp. 411–415, 2012.

[14] A. K. Verma, P. Gautam, T. N. Singh, and R. K. Bajpai, "Numerical simulation of high level radioactive waste for disposal in deep underground tunnel," in *Engineering Geology for Society and Territory Volume 1*, Springer International Publishing, Berlin, Germany, 2015.

[15] T. Wang, G. Zhou, J. Wang, and X. Zhao, "Stochastic analysis for the uncertain temperature field of tunnel in cold regions," *Tunnelling and Underground Space Technology*, vol. 59, pp. 7–15, 2016.

[16] C. Du and M. Bian, "Numerical simulation of fluid solid coupling heat transfer in tunnel," *Case Studies in Thermal Engineering*, vol. 12, pp. 117–125, 2018.

[17] L. Wang, X. Zou, H. Tao, J. Song, and Y. Zheng, "Experimental study on evolution characteristics of the heat storage of surrounding soil in subway tunnels," *Procedia Engineering*, vol. 205, pp. 2728–2735, 2017.

[18] Z. W. Li, X. T. Feng, Y. J. Zhang, C. Zhang, T. F. Xu, and Y. S. Wang, "Experimental research on the convection heat transfer characteristics of distilled water in manmade smooth and rough rock fractures," *Energy*, vol. 133, pp. 206–208, 2017.

[19] F. Kreith, R. M. Manglik, and M. S. Bohn, *Principles of Heat Transfer*, Thomson Learning, Boston, MA, USA, 1965.